JOURNAL OF MATERIALS SCIENCE **40** (2005) 5573–5580

Review Paper
Sensors development using its unusual properties of Fe/Co-based amorphous soft magnetic wire

M. HAN*, D. F. LIANG, L. J. DENG
School of Microelectronics and Solid State Electronics,University of Electronic Science and Technology of China, Chengdu, Sichuan 610054, P.R. China
E-mail: mangui@gmail.com

Published online: 25 August 2005

In this paper, the unusual properties of amorphous soft magnetic wire with Fe-based or Co-based in compositions have been discussed: giant magnetoimpedance effect (GMI), giant stress-induced impedance effect, large Barkhausen effect, magnetostriction effect. Sensor operating principles and applications exploiting these unusual properties have also been discussed: magnetic field sensors, position sensors, biosensors, non-destructive testing sensors, stress sensors etc.

1. Introduction

Since Yoshizawa *et al.* discovered $Fe_{73.5}Cu_1Nb_3Si_{13.5}B_9$ exhibited excellent behaviors of soft magnetic material [1]: high saturation magnetization, very low coercivity, very high permeability and almost zero magnetostriction, amorphous magnetic materials (in form of ribbon, thin film, rod, and bulk) have attracted a lot of attention around the world. Especially, in the past one decade, amorphous Co-based and Fe-based magnetic wire have been reported several unique behaviors due to its special domain configurations, special treatments (such as heating treatment under tension, torsion or magnetic field), and special fabrication methods: in-rotating-water quenching technique, melt-extracted method [2], Taylor-Ulitovsky method [3], Taylor method [4] (produce glass-coated wire). The commonly reported properties include giant magnetoimpedance (GMI) effect, stress-induced impedance effect, and large Barkhausen effect, magnetoelastic effects (such as Matteucci, Wiedemann and magnetostriction effects). Exploiting these special effects, many applications in sensor developments have been proposed. In this paper, a review on sensor developments using its unique effects and the underlying physics in Fe-based or Co-based amorphous magnetic wire will be discussed.

2. GMI effect

GMI effect is the most unusual property of amorphous wire. Therefore, a detailed discussion on GMI effect is given here. A GMI effect means a very large impedance change under an applied magnetic field, and has been found in amorphous wire, thin films, and ribbons. Here, we only focus on the GMI effect in an amorphous wire. A mostly used simplified circuit for GMI measurement is shown in Fig. 1. A biased DC current and a high frequency AC current (for instance $f = 10$ MHz) are applied along the longitudinal direction of an amorphous wire (usually, the diameter is about 30 μm). Both DC and AC current generate circular magnetic field around the wire and magnetize the wire transversally. When an external static magnetic field is applied along the longitudinal direction, the magnetization in the outer shell of the wire will be reoriented, and change the circumferential permeability. This result in a change in skin depth and therefore a change in impedance and in voltage between the ends of the wire will be observed. The permeability depends on many factors: domain configurations, anisotropy, stress, and magnetization modes (domain wall movement, magnetization rotation). According to the following equation, GMI effect can be expressed from the point of view of measurement on voltage change:

$$\Delta Z = \frac{\Delta V}{I} \tag{1}$$

The GMI effect also can be expressed as impedance change ratio:

$$\frac{\Delta Z}{Z}(\%) = \frac{\left[Z\left(H_{\text{ex}} = 0\right) - Z\left(H_{e_{\max}}\right)\right]}{Z\left(H_{ex_{\max}}\right)} \times 100\% \tag{2}$$

It is widely accepted that the GMI effect is due to special circumferential domain structures (see Fig. 2) in the

*Author to whom all correspondence should be addressed.
0022-2461
DOI: 10.1007/s10853-005-1462-5

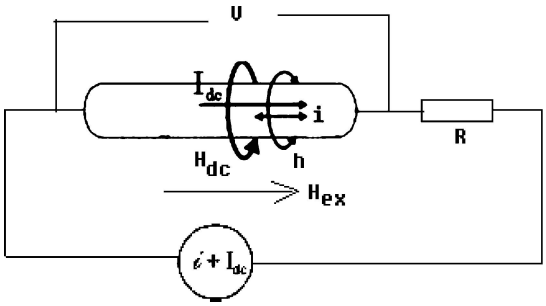

Figure 1 Schematic GMI measurement with DC-biased current I_{dc}.

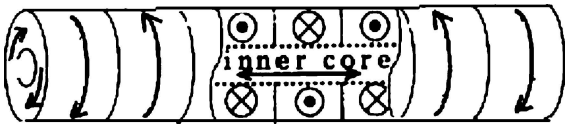

Figure 2 Domain structures of amorphous magnetic wire, the directions of magnetizations in the inner shell are parallel to the longitudinal direction; the direction of magnetization in the outer shell is circumferential.

outer shell of wire and the change of permeability by the action of external applied magnetic field. Circumferential domain configuration is the result of negative magnetostrictive constant and the residual stress distributions on the cross section of amorphous wire during its fabrication process. The complex impedance Z ($Z = R + jX$) of wire is expressed as [5]:

$$Z = \frac{R_{dc} k a B_{b0}(ka)}{2B_{b1}(ka)} \tag{3}$$

Where $k = (1+j)\,a/\delta$, $\delta = (\rho/(\mu\pi f))^{1/2}$, $\mu_\psi = \mu'_\psi - j\mu''_\psi$, R_{dc} is the dc resistance of wire, δ is the skin depth, a is the diameter of wire, ρ is the resistivity of wire, μ_ψ is the circumferential magnetic permeability of magnetic wire. $B_{b0,}$ B_{b1} is the first order of Bessel function. In order to obtain a GMI effect, the frequency of AC current should be large enough so that a strong skin effect can be obtained ($\delta \ll a$), and magnetic domain structure should ensure the permeability is sensitive to the external magnetic field.

Nowadays, a GMI effect was found about 420% in commercial Vitrovac® 6025 $Co_{67}Fe_4Mo_{1.5}Si_{16.5}B_{11}$ [6], a theoretical limit of GMI effect was reported as 10^4% [7]. A typical GMI effect curve with different frequency of an exciting AC current is given as following [8], where V_0 is related to the impedance change between the ends of wire:

At low frequency (from zero up to about 10 kHz), MI effect is mainly due to the large Barkhausen jump in the circular magnetization, and reactance X makes most contribution to the impedance change. The skin effect in this frequency range is very weak. When the frequency is within the range: 10 kHz $< f <$ 1 MHz, GMI mostly originates from the variation of skin depth which is due to strong changes of the magnetic permeability under the action of the applied static magnetic field. In this range, it is magnetization process completed by domain wall movement and magnetization rotation that contributes to the change of the circumferential permeability, only one peak is observed in the curve of Fig. 3. When f is from 1 MHz to a few

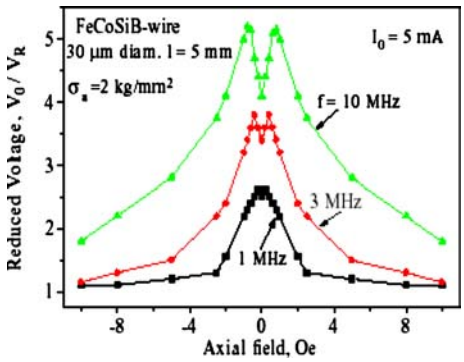

Figure 3 Typical GMI effect found in an amorphous FeCoSiB wire, from ref. [8].

hundreds MHz, GMI is mostly due to the magnetization rotation, while the domain walls movements are strongly damped by eddy currents. Two peaks in curve are found in this frequency range or even higher frequency range, see Fig. 3. When f is in order of GHz, GMI effect is due to the gyromagnetic effect and the ferromagnetic relaxation, which strongly affect the process of magnetization rotation. In this frequency range, the impedance maxima are shifted to higher magnetic fields [9].

Exploiting its GMI effect, Fe/Co-base amorphous wire can find a lot of applications in developing magnetic sensors: magnetic field sensor [10], position sensor, and biosensor. Here, discussions are given to show how these sensors were developed by exploiting GMI effect of amorphous magnetic wires.

2.1. Magnetic field sensor

Generally, sensors for measuring the magnetic field include flux gate sensor, Hall sensor, induction coil, GMR sensor, and SQUID sensor. Developing magnetic sensor using GMI effect is based on the relation: $Z \propto \sqrt{\omega\mu_\varphi H_{ex}}$. Due to advantages for GMI magnetic field sensors: high sensitivity and quick response under low magnetic field, more attentions have been paid on developing GMI magnetic field sensors. Table I illustrates the differences between GMI magnetic field sensors and other magnetic field sensors.

2.2. Position sensor

Using GMI effect, Valenzuela *et al.* have proposed a model for position sensor [15], as shown in Fig. 4. It consisted of a moving vehicle (MO) with a permanent magnet (PM) on it, a signal generator (SG) which send an ac current of 10 mA at a frequency of 100 kHz through it, a detecting circuit (D). When MO is moving, the position sensor with GMI amorphous wire can detect the variation of the magnetic field of PM. The relationship between the generated voltage of GMI sensor and the distance is shown in Fig. 5. Therefore, the position of MO can be detected. As MO approaches to the sensor, the voltage is decreased. By checking whether the voltage is less than a predetermined voltage, which is determined by the nearest distance between "W" and "PM", we can detect whether the MO is passing the sensor. Similar position sensor development was also

TABLE I Comparison of magnetic field sensors commonly used

	H range (Tesla) [11]	Sensitivity (V/Tesla)[12]	Response time [14]	Power consumption [14]	Sensor head size
GMI	10^{-11}–10^{-4}	4600	1 MHz	10 mw	1–2 mm
GMR	10^{-12}–10^{-2}	120	1 MHz	10 mw	10–100 μm
Hall	10^{-6}–10^{2}	0.65	1 MHz	10 mw	10–100 μm
SQUID	10^{-14}–10^{-6}	10^{-14} [13]	1 MHz	10 mw	10–100 μm
Flux gate	10^{-12}–10^{-2}	3.2	5 kHz	1 w	10–20 mm

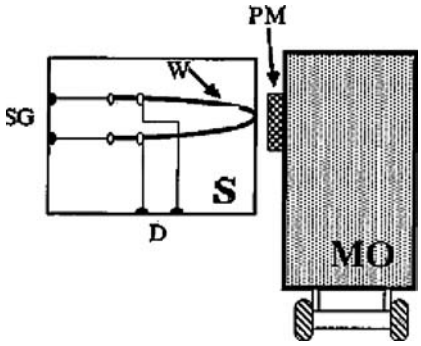

Figure 4 Operating principle of a GMI position sensor (S), a magnetic wire (W), a signal generator (SG), a permanent magnet (PM), a moving vehicle (MO), a detecting circuit (D), from ref. [15].

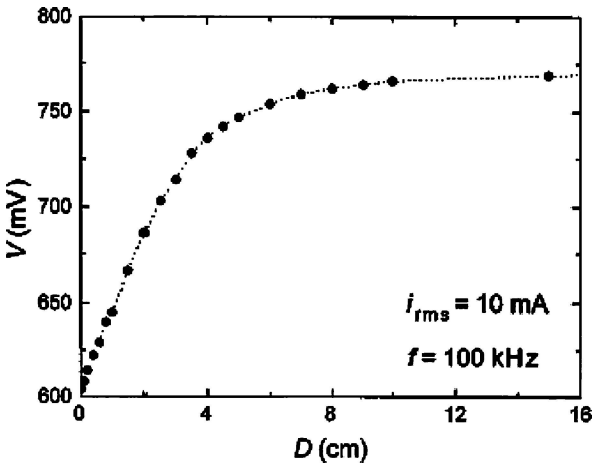

Figure 5 Relationship between the distance and voltage for the GMI sensor, from ref. [15].

reported in $(Co_{0.94}Fe_{0.06})_{72.5}Si_{12.5}B_{15}$ amorphous wire by Atalay *et al*. [16].

Another example of position sensor developed in Japan is a magnetic tracking system using a GMI sensor, as shown in Fig. 6. On highway, magnetic markers (with amorphous magnetic wire inside) are embedded on highway, a GMI sensor on the head of car is used to sense the position of markers. This information is then fed into a microcontroller in the car. Consequently, the position of car on the highway can be controlled without the participation of driver [17].

2.3. Biosensor

In modern medical therapy, doctors often need to access the diseased areas (such as blood vessel, branch of bronchus, stomach, and duodenum) by inserting a catheter. X-ray radioscopy is often used in many hospitals to monitor the position and orientation of the inserted catheter, but due to the fact that it has a negative effect on patient and medical staff, there is a need to find a more subtle and less harmful sensor which can image the orientation of catheter in a patient's body. GMI sensor has some advantage over other sensor, such as lower power consumption (10 mW), sensitivity (10^{-10} Tesla), high response speed (10 MHz), and small size (<2 mm). It can satisfy requirements for catheterization. Totsu *et al*. have investigated the application of GMI sensor in catheter navigation system [18], the operating principle is shown in Fig. 7. The 2-axis source coil near a patient is used to emit an AC magnetic field, the earth's magnetic field is the source of DC magnetic field for GMI sensor. The *x*-*y*-*z* orthogonal sensor is detecting the GMI signal from the tip of catheter. After signals processing in computer, the images of catheter orientations are shown on screen for doctor. GMI sensor is installed on the tip of a polymer tube, as shown in Fig. 8, the GMI sensor size is about 1 × 1 × 1 mm.

GMI has also been employed to develop the sensor to detect position and 3D images of a tumor in brain using a micro magnetoimpedance sensor and fine magnetic particles (Fe_3O_4 with an average diameter of 25 nm) dispersed in a gel sample [19]. It was found that the monoclonal antibody is conjugated with magnetic particle coated with polyethylene glycol, and the coated magnetic particles have a tendency to accumulate in a tumor issue. Therefore, by sensing the spatial distribution of stray field of magnetic particles, the position and 3D image of a tumor can be obtained.

To further improve the sensor linearity and temperature stability for the GMI magnetic field sensors, the asymmetric and off-diagonal MI effects have been employed to develop magnetic field sensor with higher performances [20, 21]. To obtain an asymmetric MI characteristic, a helical anisotropy is required which can be achieved by annealing under torsion [22], for more detailed information, interested readers can refer to these papers.

3. Stress-induced impedance effect and sensor

It is reported that the impedance of magnetic wire is also a function of applied stress, as shown in Fig. 9 for $Co_{68.5}Mn_{6.5}Si_{10}B_{15}$ amorphous microwire with 16.5 μm. When tensile stress is increased, the maximum field H_{max} corresponding to the maximum GMI ratio ($\Delta Z/Z$) is linearly shifted to higher value, as shown in the inset in Fig. 9.

It was proposed that the dependence of GMI ratio on the tensile stress is because that the tensile stress introduces a magnetoelastic (ME) anisotropy, $H_{k.}$ It is well known that the ME anisotropy plays a critical role

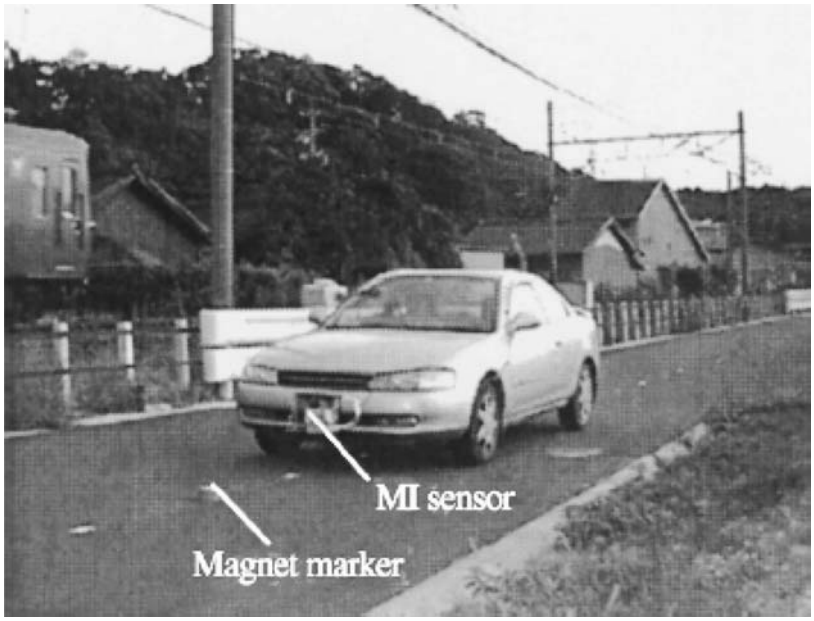

Figure 6 Magnetic tracking system using GMI sensor, from ref. [17].

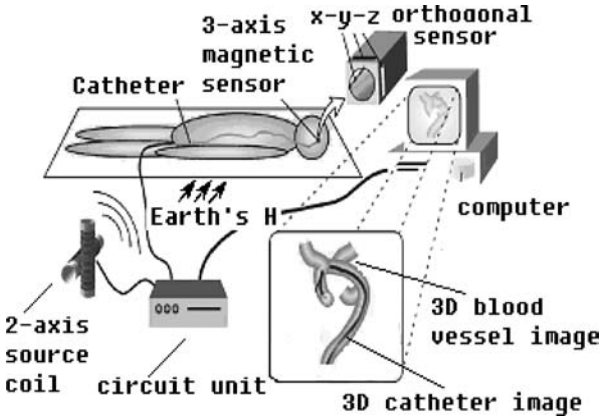

Figure 7 Operation principle of a 3-D GMI sensor system using for catheterization, from ref. [18].

in determining the magnetization direction by the sign of $\lambda\sigma$: if $\lambda\sigma > 0$, M direction is parallel to the direction of the applied stress σ when it is saturated into a single domain structure. Based on the linear relationship between the applied stress and maximum field $H_{\max}$, a stress sensor can be implemented [24], as shown in Fig. 10. Where one end of the microwire with GMI effect is fixed, the other end is connected to a sail which can be moved by the applied stress. Such a sensor can be used in areas which need to measure small mechanical stress. It is also reported that the SI sensor using $Co_{72.5}Si_{12.5}B_{15}$ ($\lambda s = -3 \times 10^{-6}$) amorphous wire has a strain-gauge factor more than 2000, which is more than 10 times larger than that of a semiconductor strain gauge [25].

4. Non-destructive testing (NDT) sensor

Barkhausen effect in ferromagnetic materials is often used to develop NDT sensor system. Barkhausen effect is often observed in the magnetization process of ferromagnetic materials. The physics underlying is the discontinuous magnetization change due to the irreversible movements of domain walls and irreversible rotation of magnetization under external applied stress or magnetic field, as shown in Fig. 11 for ordinary ferromagnetic materials.

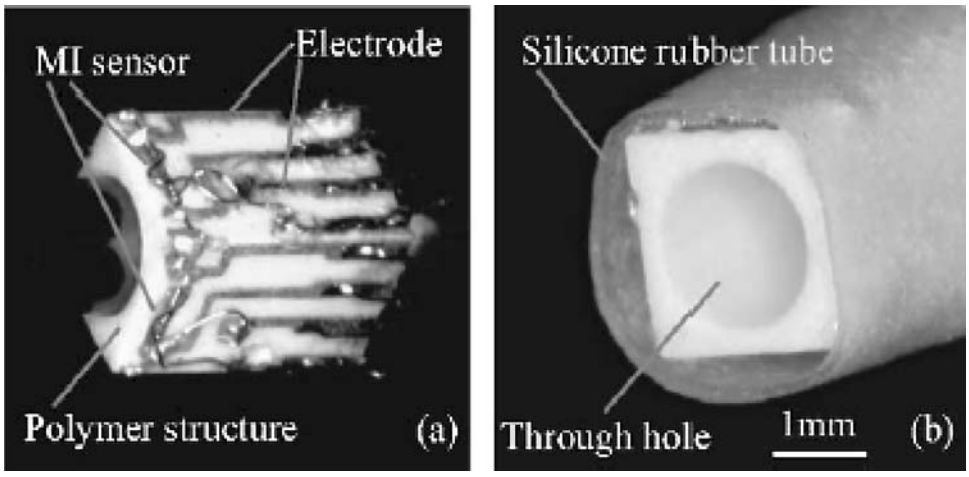

Figure 8 A 3-D GMI sensor (size: 1 × 1 × 1 mm) on a tiny polymer tuber, from ref. [18].

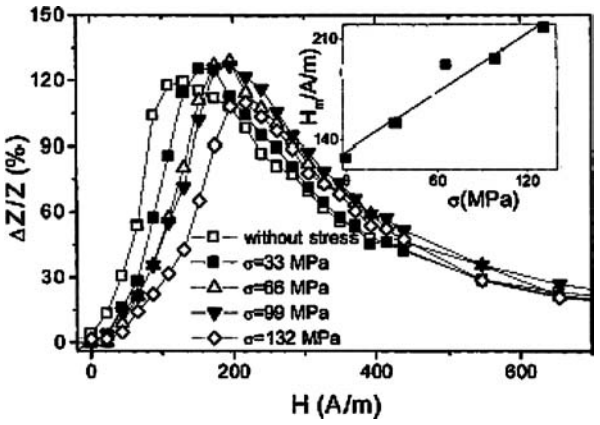

Figure 9 Dependence of GMI ratio on the applied tensile stress, ac current is 1.5 mA at a frequency of 10 MHz for $Co_{68.5}Mn_{6.5}Si_{10}B_{15}$ amorphous wire. The inset shows the dependence of H_m on tensile stress, from ref. [23].

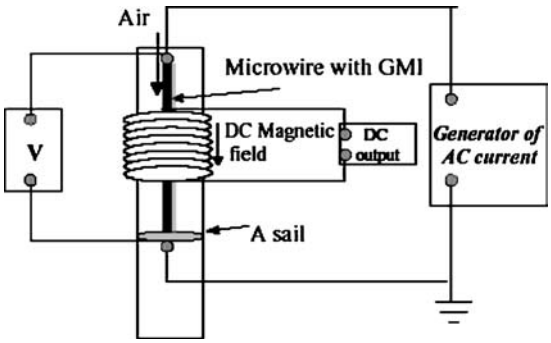

Figure 10 Stress sensor based on stress-induced impedance effect, from ref. [24].

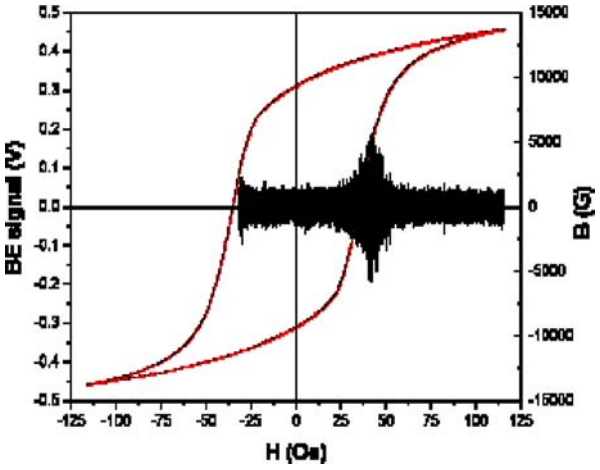

Figure 11 Barkhausen Effect and Barkhausen signal, from ref. [26].

The inner cylinder core of amorphous magnetic wire has a domain structure where only 180° domain axially oriented. Under external applied magnetic field, the magnetization which direction is opposite to the direction of the applied magnetic field will "jump" to the direction of magnetic field at some critical magnetic fields. For $Co_{68.5}Mn_{6.5}Si_{10}B_{15}$ amorphous wire [27], its M-H curve is a square loop, which can produce a large Barkhausen signal. Therefore, exploiting its large Barkhausen effect, amorphous magnetic wire can be used to develop non-destructive sensors: when there are some imperfections (crack, internal residual stress, non-magnetic inclusions) in ferromagnetic material (such as low carbon steel), the magnetic field on surface of magnetic material will be inhomogeneous, and amorphous magnetic wire sensor can detect the variation of magnetic field, then the distribution information of imperfections in material can be obtained. Besides the Barkhausen effect, GMI effect in amorphous wire was also exploited to develop NDT sensor. Goktepe *et al*. have developed a NDT sensor using $(Co_{0.96}Fe_{0.04})_{72.5}Si_{12.5}B_{15}$ amorphous wire to detect cracks in a ferromagnetic material [28], as shown in Fig. 12a and b, (a) shows the operation principle of sensor, (b) shows the sensor output for a sample with a crack and a sample without a crack. GMI sensor also has been used to investigate the microstructures in a pressure vessel: grain size, carbide morphology, lath wide, lath boundary [29].

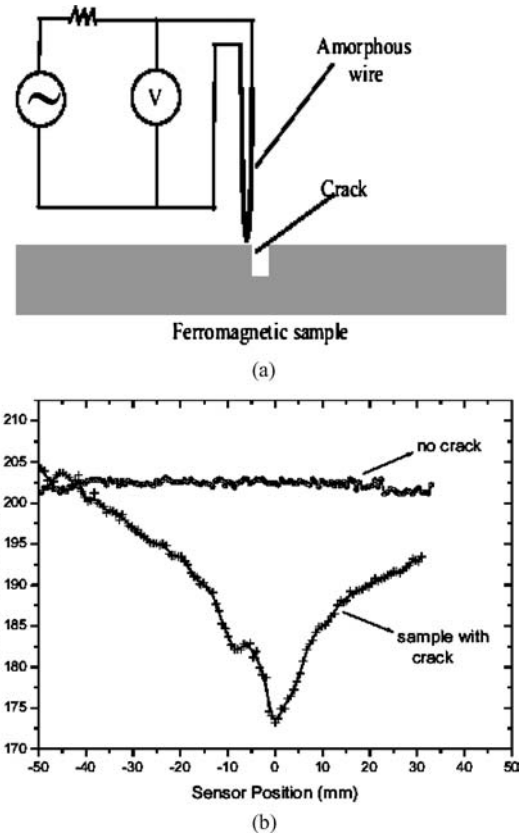

Figure 12 GMI non-destructive sensor using amorphous wire $(Co_{0.96}Fe_{0.04})_{72.5}Si_{12.5}B_{15}$, (a) shows the operation principle of NDT sensor, (b) shows the differences in sensor output for samples with and without cracks, from ref. [28].

5. Electronic article surveillance

The B-H shape loop of Fe-base wire can be square, if the wire properly fabricated. As shown in Fig. 13a for $Co_{72.5}Si_{12.5}B_{15}$ amorphous wire [30]. If the tag containing a magnetic wire is attached to an item and not deactivated, when it pass through the exit, it is excited by a magnetic field (from the transmitter installed at exit) with a predetermined frequency, and will generate a magnetic wave with higher harmonics, which can be detected by a receiver installed at exit and trigger the alarm. This is the operating principle of EAS tag with a single bit. A multi-bit EAS system usually has a coding/decoding feature so that a number of articles

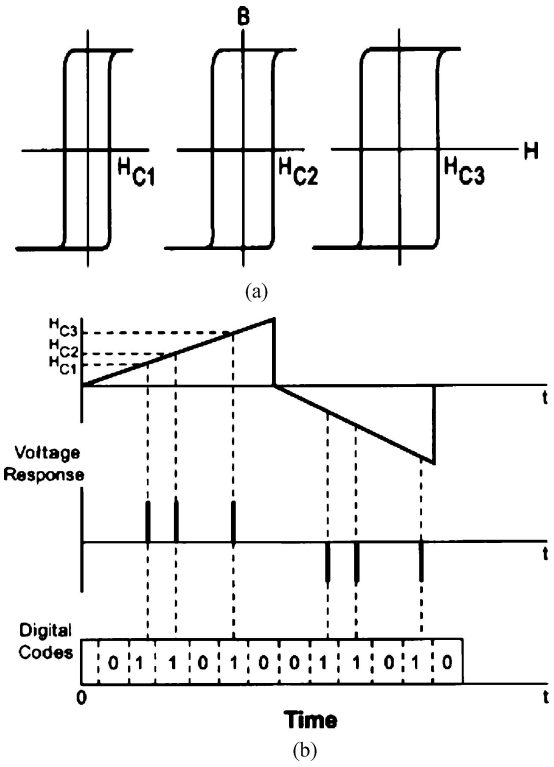

Figure 13 (a) Magnetic wires with different coercivity in a multi-bit EAS system, from ref. [30]. (b). The operating principle of multi-bit EAS system, from ref. [30].

can be identified. To do this, a number of magnetic markers (wires) with different coercivity are included in an EAS system, as shown in Fig. 13a.

When an applied magnetic field with a time-dependent profile as shown above in Fig. 13b, the voltage responses generated by the wires are shown in the middle of Fig. 13b, then the voltage responses can be converted into digital codes, as shown in the bottom of Fig. 13b.

6. Magnetostrictive sensors

6.1. Position sensor using ultraacoustic standing wave

Usually, the magnetostriction is pretty small for Co-based (negative) amorphous glass-coated wire [31]

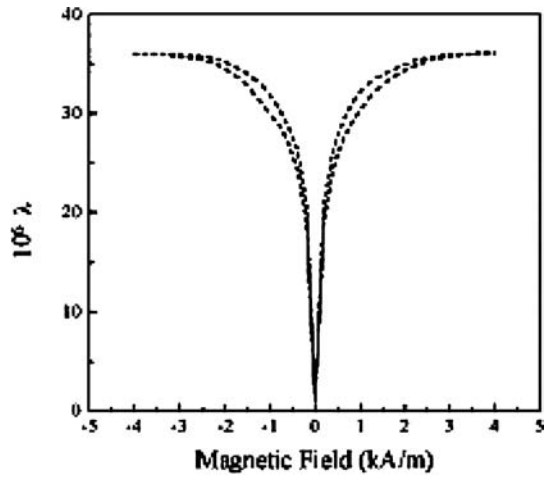

Figure 14 Magnetostriction of amorphous $Fe_{77.5}Si_{7.5}B_{15}$ wire with large $d\lambda/dH$ value in low field, from ref. [33].

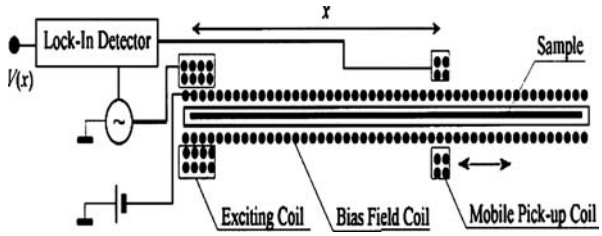

Figure 15 Position sensor based on ultraacoustic standing wave in amorphous $Fe_{77.5}Si_{7.5}B_{15}$ wire, from ref. [33].

(such as $Co_{68.5}Fe_{4.35}Si_{12.5}B_{15}$ with $\lambda s = -1.11 \times 10^{-7}$), and Fe-based amorphous glass-coated wire [32], such as $Fe_{72.5}Si_{12.5}B_{15}$ ($\lambda s = 32 \times 10^{-6}$). For FeSiB amorphous wire, due to its large change rate of magnetostriction with respective to the small applied magnetic field, i.e., $d\lambda/d$H, it has been used to develop magnetoelastic sensors, one example is to develop a position sensor using its ultraacoustic standing wave, as shown in Fig. 14. Under an applied magnetic field, the wire will be deformed along the longitudinal direction, a sinusoidal magnetic field induces a sinusoidal mechanical wave. Under some conditions, a mechanical wave in wire produces an ultraacoustic wave [33]. In Fig. 15, where the exciting field is used to produce a sinusoidal magnetic field, the bias field is produce by a DC current coil, To obtain ultraacoustic standing wave, the signal generator controls the reference signals for the lock-in detector, which is connected with a mobile pick-up coil along the wire axis to determine the position x. The relationship between the position and the induced signal can be expressed as:

$$V = V_0 \sin\left(\frac{\pi \cdot x}{L}\right) \tag{4}$$

where L is the wire length, x is the position of pick-up coil along the wire, V_0 is a constant. The accuracy of this sensor can be higher than 10^{-4} m.

6.2. Magnetostrictive delay line (MDL) sensor

Differing from the domain structure mentioned in Fig. 2, for Fe-rich amorphous wire ($Fe_{77.5}Si_{7.5}B_{15}$), its domain structure is shown in Fig. 16 below. When applying a DC bias magnetic field (the moving permanent magnet as shown in Fig. 17) along the axis of wire, the magnetizations in the outer shell of domain will rotate toward the direction of magnetic field, resulting in a deformation in the outer shell (magnetostriction effect). For the inner shell, since domain structure is 180° domain wall, no magnetostriction is resulted. If a pulse magnetic field (see the exciting coil in Fig. 17) is applied at the same region as the DC magnetic field, a time-dependent magnetostriction will be superimposed in the previous one. The total time-varying magnetostriction is maximum on the surface of wire and decays gradually towards the inside core, and generating a longitudinal elastic wave, called surface acoustic wave (SAW) propagating along the wire. If receiving coils are installed at the ends of wire, a pulsed

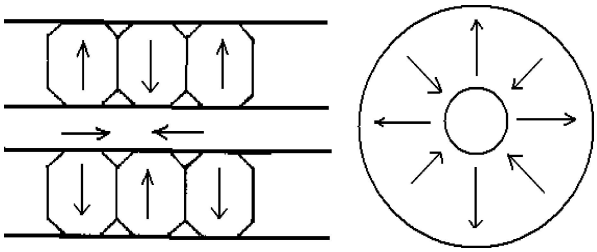

Figure 16 Domain structure for Fe-rich amorphous wire.

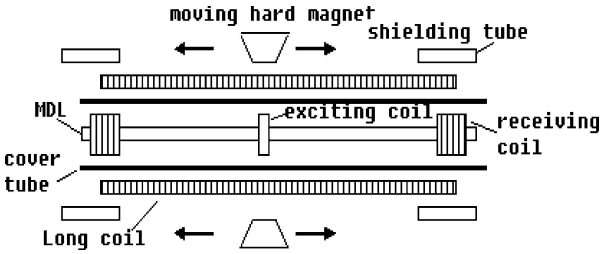

Figure 17 Cordless position sensor based on the MDL principle, from ref. [34].

voltage will be induced based on inverse magnetostriction effect in the receiving coils, the induced voltage is proportional to the distance between the moving magnet and the receiving coil. Based on this principle, the position sensor can be developed.

MDL sensor also can be used in sport field, such as detecting the height of jump, the distance of triple jump accurately [35], force sensor [36], digitizer [37], nondestructive sensor [38] et al. by modifying and controlling the factors which affect the MDL characteristics: such as frequency of exciting field, force exerting on wire, bias field.

7. Conclusions

Amorphous wires of Co-based with negative magnetostriction and Fe-based with positive magnetostriction finds wide applications in sensor development, including magnetic sensors, stress sensors, torque sensors, position sensors, NDT sensors, biosensors etc. More and more sensors have been reported using amorphous soft magnetic wire when more interesting properties are found (such as Matteucci effect [39–41], Wiedemann effect [42–44], ferromagnetic resonance effect [45–47], and Kerr effect [48]), and when more subtle controls on the characteristics of materials are available.

References

1. Y. YOSHIZAWA, S. OGUMA and K. YAMAUCHI, *J. Appl. Phys.* **64** (1988) 15.
2. P. RUDKOWSKI, G. RUDKOWSKA and J. O. STROMOLSEN, *Mater. Sci. Eng. A* **133** (1991) 158.
3. USSR patent, No.128427.
4. H. CHIRIAC and T. A. OVARI, *Prog. Mater. Sci.* **40** (1996) 33.
5. M. KAMRUZZAMAN, I. Z. RAHMAN and M. A. RAHMAN, *J. Mater. Proc. Tech.* **119** (2001) 312.
6. G. V. KURLYANDSKAYA, V. M. PRIDA, B. HERNANDO, J. D. SANTOS, M. L. SÁNCHEZ and M. TEJEDOR, *Sens. Act. A* **110** (2004) 228.
7. L. KRAUS, *J. Magn. Magn. Mater.* **196** (1999) 354.
8. L. V. PANINA, D. P. MAKHNOVSKIY and K. MOHRI, *J. Magn. Magn. Mater.* **272** (2004) 1452.
9. L. KRAUS, *Sens. Act. A* **106** (2003) 187.
10. A. E. MAHDI, L. PANINA and D. MAPPS, *ibid.* **105** (2003) 271.
11. *Idem., ibid.* **105** (2003) 271.
12. U. BARJENBRUCH, *Sens. Act. A* **65** (1998) 136.
13. A. E. MAHDI, L. PANINA, and D. MAPPS, *ibid.* **105** (2003) 271.
14. K. MOHRI, T. UCHIYAMA, L. P. SHEN, C. M. CAI and L. V. PANINA, *J. Magn. Magn. Mater* **249** (2002) 351.
15. R. VALENZUELA, M. VAZQUEZ and A. HERNANDO, *J. Appl. Phys.* **79** (1996) 6549.
16. F. E. ATALAY and S. ATALAY, *Phys. Stat. Sol. (a)* **189** (2002) 311.
17. Y. HONKURA, *J. Magn. Magn. Mater* **249** (2002) 375.
18. K. TOTSU, Y. HAGA and M. ESASHI, *Sens. Act. A* **111** (2004) 304.
19. T. UCHIYAMA, K. MOHRI, M. SHINKAI, A. OHSHIMA, H. HONDA, T. KOBAYASHI, T. WAKABAYASHI and J. YOSHIDA, *IEEE Trans. Magn.* **33** (1997) 4266.
20. K. MOHRI, T. UCHIYAMA, L. P. SHEN, C. M. CAI, L. V. PANINA, Y. HONKURA and M. YAMAMOTO, *IEEE Trans. Magn.* **38** (2002) 3063.
21. L. V. PANINA, *J. Magn. Magn. Mater.* **249** (2002) 278.
22. K. KAWASHIMA, I. OGASAWARA, S. UENO, K. MOHRI, *IEEE Trans. Magn.* **35** (1999), 3610.
23. A. F. COBENO, A. ZHUKOV, J. M. BLANCO, V. LARIN and J. GONZALEZ, *Sens. Act. A* **91** (2001) 95.
24. *Idem., ibid.* **91** (2001).
25. L. P. SHEN, T. UCHIYAMA, K. MOHRI and K. BUSHIDA, *IEEE Trans. Magn.* **33** (1997) 3355.
26. D. C. JILES, "Introduction to Magnetism and Magnetic Materials," 2nd edn. (Chapman and Hall, 1999.)
27. A. F. COBENO, J. M. BLANCO, A. ZHUKOV and J. GONZALEZ, *J. Magn. Magn. Mater.* **249** (2002) 402.
28. M. GOKTEPE, Y. EGE, N. BAYRI and S. ATALAY, *Phys. Stat. Sol. (c)* **1**(2) (2004) 3436.
29. D. J. KIM, D. G. PARK and J. H. HONG, *J. Appl. Phys.* **91** (2002) 7421.
30. V. ZHUKOVA, A. ZHUKOV, J. GONZALEZ and J. M. BLANCO, *J. Magn. Magn. Mater.* **254** (2003) 182.
31. H. CHIRIAC, M. NEAGU, M. VAZQUEZ and E. HRISTOFOROU, *J. Magn. Magn. Mater* **242–245** (2002) 251.
32. M. NEAGU, H. CHIRIAC and C. HISON, *Sens. Act. A* **115** (2004) 490.
33. H. CHIRIAC and C. S. MARINESCU, *Sens. Act. A* **81** (2000) 174.
34. E. HRISTOFOROU, *Sens. Act. A* **59** (1997) 183.
35. E. HRISTOFOROU and H. CHIRIAC, *J. Magn. Magn. Mater* **249** (2002) 407.
36. E. HRISTOFOROU, H. CHIRIAC, M. NEAGU, I. DARIE and A. OVARI, *IEEE Trans. Magn.* **32** (1996) 4953.
37. E. HRISTOFOROU and R. E. REILLY, *IEEE Trans. Magn.* **28** (1992) 1974.
38. E. HRISTOFOROU, D. NIARCHOS, H. CHIRIAC and M. NEAGU, *Sens. Act. A* **92** (2001) 132.
39. V. M. PRIDA, B. HERNANDO, M. L. SÁNCHEZ, Y. F. LI, M. TEJEDOR and M. VÁZQUEZ, *J. Magn. Magn. Mater.* **258/59** (2003) 158.
40. V. RAPOSO, M. VÁZQUEZ and A. MITRA, *ibid.* **254/55** (2003) 179.
41. B. HERNANDO, V. M. PRIDA, M. L. SÁNCHEZ, M. TEJEDOR, M. VÁZQUEZ and L. Y. FENG, *ibid.* **254/55** (2003) 525.
42. H. CHIRIAC, C. S. MARINESCU and M. MARINESCU, *ibid.* **196/97** (1999) 367.
43. J. J. FREIJO, M. VAZQUEZ, A. HERNANDO, A. MENDEZ and V. R. RAMANAN, *J. Appl. Phys.* **85** (1999) 5450.

44. A. F. COBENO, A. ZHUKOV, J. M. BLANCO and J. GONZALEZ, *Sens. Act. A* **106** (1–3) (2003) 174.
45. V. A. TULIN, M.V. ASTAHOV and A. O. RODIN, *J. Magn. Magn. Mater.* **258/259** (2003) 201.
46. R. S. DE BIASI and W. S. D, *Folly, Phys. B* **321** (1–4) (2002) 117.
47. C. GÓMEZ-POLO, J. M. BARANDIARÁN and J. GUTIÉRREZ, *Sens. Act. A* **106** (1–3) (2003) 155.
48. V. ZHUKOVA, A. ZHUKOV, J. GONZALEZ and M. BLANCO, *Magn. Mater.* **254/255** (2003) 182.

Received 25 January
and accepted 13 April 2005